We are IntechOpen, the world's leading publisher of Open Access books Built by scientists, for scientists

4,800
Open access books available

122,000
International authors and editors

135M
Downloads

Our authors are among the

154
Countries delivered to

TOP 1%
most cited scientists

12.2%
Contributors from top 500 universities

CLARIVATE ANALYTICS BOOK CITATION INDEX INDEXED

WEB OF SCIENCE™

Selection of our books indexed in the Book Citation Index in Web of Science™ Core Collection (BKCI)

Interested in publishing with us?
Contact book.department@intechopen.com

Numbers displayed above are based on latest data collected.
For more information visit www.intechopen.com

16

Unidirectional feeding of submillimeter microparts along a sawtooth surface with horizontal and symmetric vibrations

Atsushi Mitani[1] and Shinichi Hirai[2]
[1]*Department of Design, Sapporo City University*
[2]*Department of Robotics, Ritsumeikan University*
Japan

1. Introduction

Devices to feed along microparts, such as ceramic chip capacitors and resistors, have become more common, due to their use in sorting, inspecting, and shipping mass produced microparts. In microparts feeding, to feed along microparts in one direction, the driving force applied to each micropart must vary according to the direction of movement of the micropart. Especially, the movement of microparts smaller than submillimeter can be affected not only inertia but also adhesion which is caused by electrostatic, van der Waal's, intermolecular, and surface tension forces (Ando, 1997). Therefore, we need to derive dynamics including adhesion to evaluate the movement of microparts.

We have previously shown that a sawtoothed surface with simple planar and symmetric vibrations can be used to feed along microparts (Figure 1) (Mitani, 2006). In this case, contact occurs in one of two ways: point contact, the point of the tooth contacts the fed part, and slope contact, the sloping side of the tooth contacts the micropart. Because of the difference in contact area of micropart with the sloping side of a tooth and with the other side, microparts adhere more strongly in one direction than in the other. Also, the driving forces transferred from vibrations of feeder surface vary according to contact. These result in the microparts moving in one direction with simple planar symmetric vibrations.

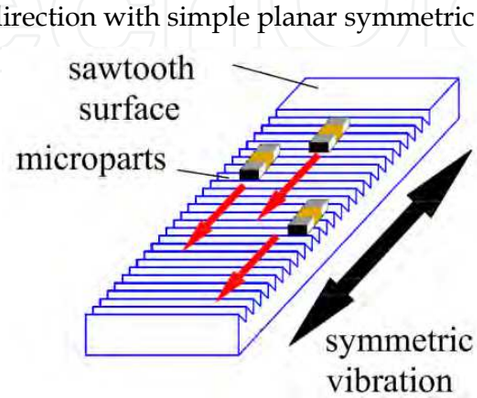

Fig. 1. Diagram of microparts feeding using a sawtoothed surface

We assessed the effect of sawtoothed silicon wafers for feeding of 0603 capacitors (size, 0.6 x 0.3 x 0.3 mm: weight, 0.3 mg). Using these experimental results, we verified relationship among feed velocity, driving frequency, and sawtooth pitch. Analysing contact between feeder surface and a micropart based on measurements using a microscope, we developed feeding dynamics including adhesion. Comparing experiments with feeding simulation using the dynamics derived, we found large errors between both results. To examine these errors, we observed the movement of a micropart when the micropart moved in one direction using a high speed video camera. We then found that the micropart rotated around vertical axis against the feeder surface and swung around the axis parallel to the tooth groove, thus reductions of feed velocity occurred. Consequently, the feeding dynamics considering these movements were needed for more accurate simulations.
The objective of this work was to examine the dynamics of microparts tens or hundreds of micrometers in size. We found that the movement of these parts depends on both inertia and adhesion.

2. Related Works

Partsfeeder is a key device in factory automation. The most popular feeders are vibratory bowl feeders (Maul, 1997), which use revolving vibrators to move parts along a helical track on the edge of a bowl. Linear feeders as well as an inclined mechanism and oblique vibration for unidirectional feeding (Wolfsteiner, 1999), have also been developed. In all of these systems, the aspect ratio of the horizontal/vertical vibrations must be adjusted to prevent parts from jumping. In our system, however, this adjustment is not necessary because only horizontal vibration is used.
A parts feeding that employs non-sinusoidal vibrations (Reznik, 2001) has been developed. The part moves to its target position and orientation or is tracked during its trajectory by using the difference between the static and sliding friction. Our system realizes unidirectional feeding by symmetric vibration of a sawtoothed surface, which yields different contact forces in the positive and negative directions.
Designing have been tested by simulation (Berkowitz, 1997 & Christiansen, 1996). The focus was mainly on the drive systems such as the structure and actuator, the movement of fed parts was generally neglected. In contrast, the movement of the microparts are considered in the present study.
Attempts have been made to improve the drive efficiency by feedback control systems (Doi, 2001) and nonlinear resonance systems (Konishi, 1997). Our system depends only upon contact between the feeder surface and the micropart. So the driving system is simple and uses an open loop system for feeding.
Micro-electro-mechanical systems (MEMS) technology has been used to mount on a planar board arrays of micro-sized air nozzles which, by turning on or off their air flow, have been used to control the direction of moving microparts (Fukuta, 2004 & Arai, 2002).
It is possible to perform manipulation with ciliary systems (Ebefors, 2000) and vector fields (Oyobe, 2001) without sensors. In this case, there are many actuator arrays on a vibratory plate. Actuator arrays enable control of contact between the vibratory plate and micropart in order to accomplish the target manipulation. However, these studies did not mention the dynamics of the micropart, especially the effects of adhesion forces on its motion. Other various feeding systems using electric-field (Fuhr, 1999), magnetic (Komori, 2005), bimorph

piezoelectric actuators (Ting, 2005), and inchworm systems (Codourey, 1995) have been developed. These studies, however, have also not investigated the contact between the feeder surface and the micropart.

3. Principe of unidirectional feeding

Let us first look at a typical micropart, a 0603 ceramic chip capacitor used in electronic devices (Figure 2). Then let us analyse feeding by developing a model for contact between a micropart and a sawtooth.

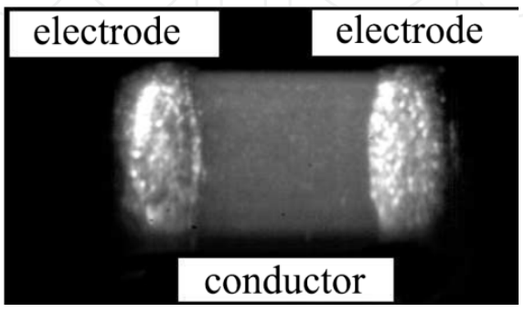

Fig. 2. Ceramic chip capacitor 0603 (size, 0.6 x 0.3 x 0.3 mm: weight, 0.3 mg)

A capacitor consists of a conductor and electrodes with convexities on each end surface. We obtained representative contours along a capacitor using a Form Talysurf S5C sensing-pin surface measurement tool (Taylor Hobson Corp.) (Figure 3). Electrodes contact the feeder because they protrude 10 μm higher than the conductor.
Assuming that convexities are perfectly spherical (Figure 4 (a)), let r be the radius of a convexity (Figure 4 (b)). The feeder surface is sawtoothed (Figure 5), let θ be sawtooth elevation angle, p sawtooth pitch, and d the groove depth. The sawtooth contacts the electrode in one of two ways (Figure 6) - at the tooth point or at the tooth slope. To drive the microparts unidirectionally, driving must depend on the contact and direction of movement.

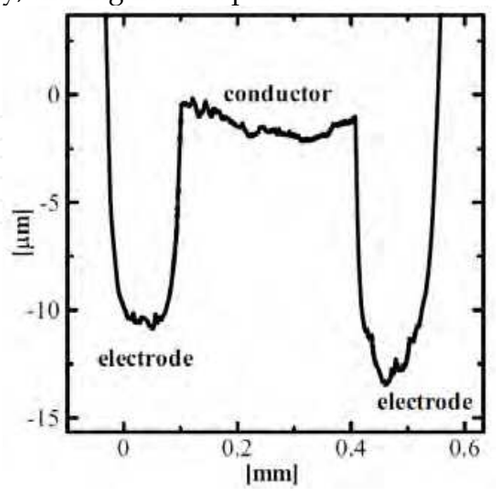

Fig. 3. A section of 0603 capacitor

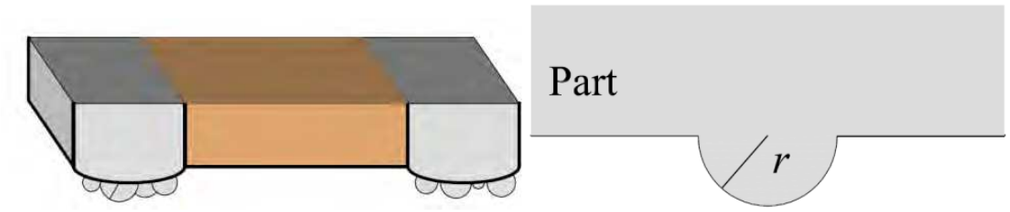

(a) surface model (b) convexity

Fig. 4. Model of surface convexity on an electrode

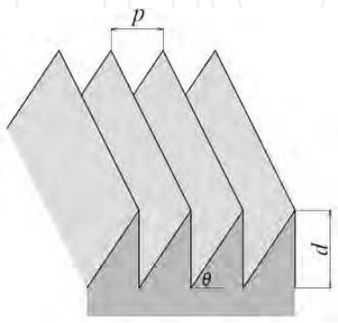

Fig. 5. Model of sawtooth surface

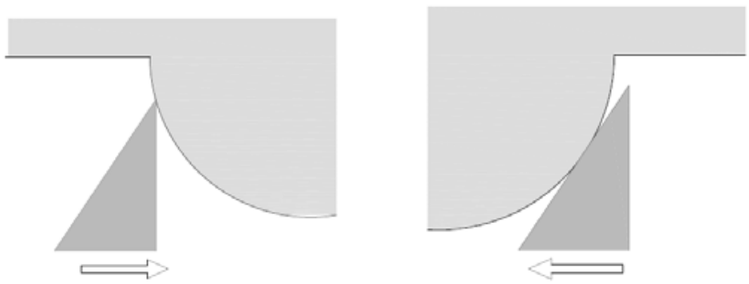

(a) at tooth point (b) at tooth slope

Fig. 6. Two contacts between micropart and sawtooth

4. Feeding experiments of 0603 capacitor

4.1 Experimental equipments

In micropart feeder (Figure 7), a silicon wafer is placed at the top of the feeder table, which is driven back and forth in a track by a pair of piezoelectric bimorph elements, powered by a function generator and an amplifier that delivers peak-to-peak output voltage of up to 300 V.

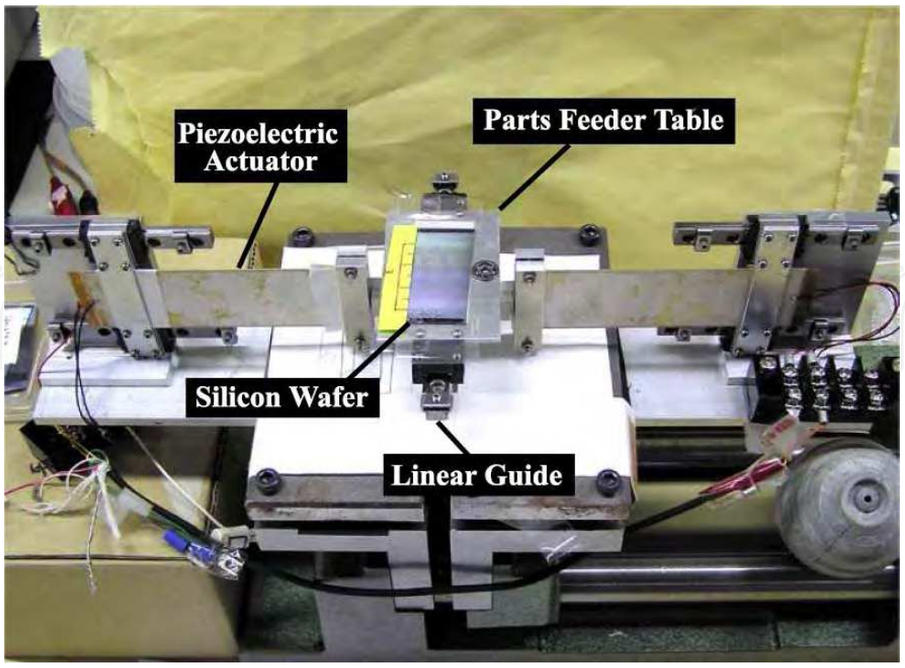

Fig. 7. Microparts feeder using bimorph piezoelectric actuators

4.2 Sawtooth surfaces

We used a dicing saw (Disco Corp.), a high-precision cutter-groover using a bevelled blade to cut sawteeth in silicon wafers. Figure 8 shows a microphotograph of a cut silicon wafer with sawteeth of $p = 0.1$ mm, $\theta = 20$ deg, and $d = p \tan \theta = 0.0364$ mm. We prepared sawtoothed silicon wafers with pitch $p = 0.01, 0.02, \cdots, 0.1$ mm and elevation angle $\theta = 20$ deg.

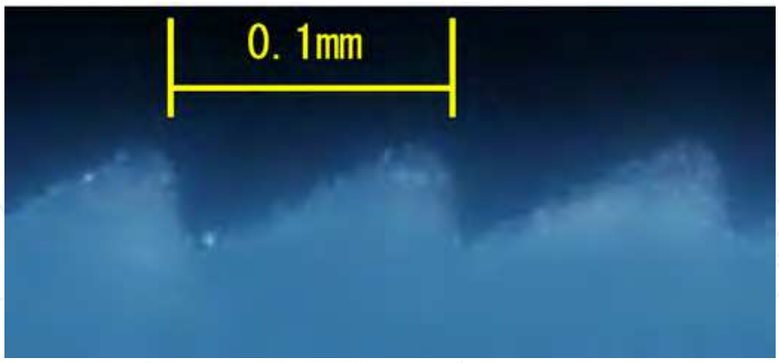

Fig. 8. Microphotograph of a sawtoothed silicon wafer

4.3 Experiments

Using the microparts feeder and these sawtoothed surfaces, we conducted feeding experiments with 0603 capacitor. Micropart movement was recorded using a digital video camera at 30 fps. Velocity was measured by counting how many frames it took for a micropart to move 30 mm along the sawtooth surface. Microparts moved at a drive

frequency f = 98 to 102 Hz and feeder table amplitude was about 0.20 mm. Each value is the average of three trials, each trial using five capacitors (Figure 9).

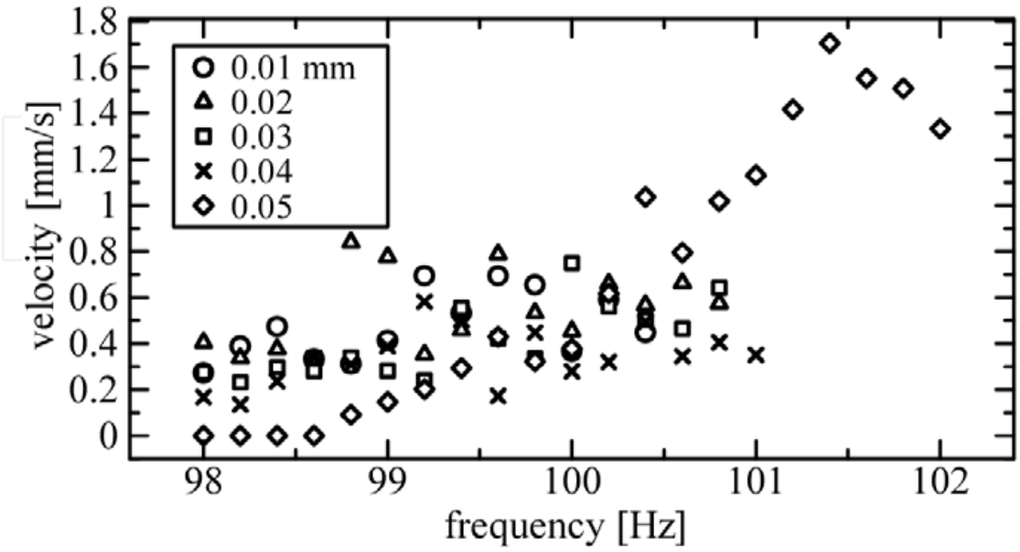

(a) p = 0.01 to 0.05 mm

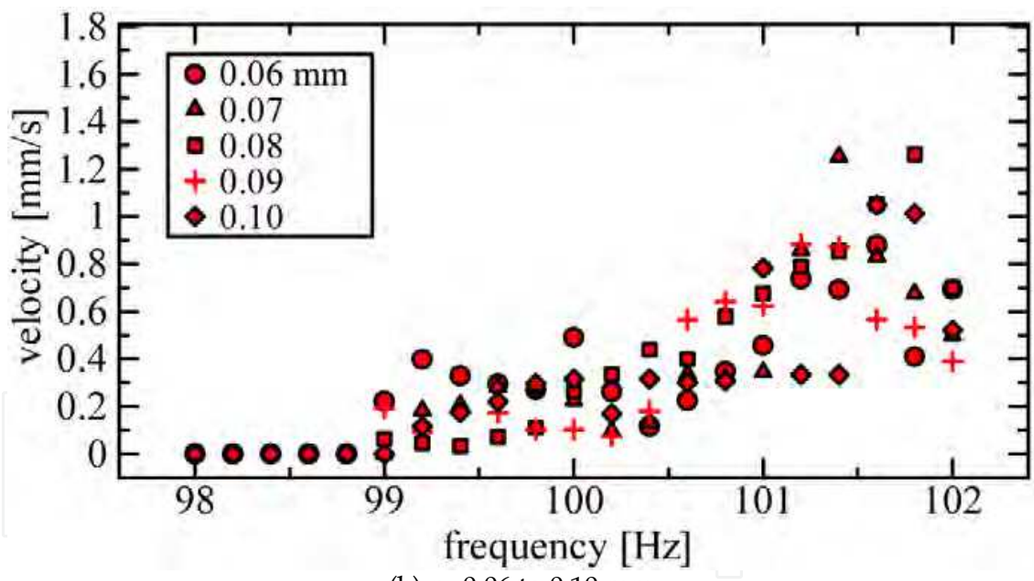

(b) p=0.06 to 0.10 mm

Fig. 9. Experimental results of 0603 capacitor

Table 1 shows the drive frequency that realized maximum velocity for each pitch, and its maximum velocity. When the pitch was 0.04 mm or less, velocity was 0.6 mm/s at drive frequency f = 98 to 101 Hz, but movement was jittery. At higher drive frequency, the microparts jumped. Fastest feeding was 1.7 mm/s, realized at f = 101.4 Hz with p=0.05 mm. When the pitch was 0.06 mm or greater, maximum feed velocity on a surface was realized

when drive frequency was 101.4 Hz. The maximum velocity decreased with increasing pitch, indicating the appropriate pitch for 0603 capacitors is p = 0.05 mm.
Figure 9 shows velocity dispersion at the maximum feed velocity on each sawtooth surface. Feed velocity dispersed within 6.7 to 23.5 %, averaging 15.8 %. The smallest dispersion occurred at a sawtooth pitch of 0.05 mm. Consequently, the sawtooth surface with pitch p = 0.05 mm was most appropriate for feeding 0603 capacitor.

pitch, mm	velocity, mm/s	frequency, Hz
0.01	0.695	99.2
0.02	0.839	98.8
0.03	0.749	100.0
0.04	0.582	99.2
0.05	1.705	101.4
0.06	0.880	101.6
0.07	1.253	101.4
0.08	1.262	101.8
0.09	0.883	101.2
0.10	1.049	101.6

Table 1. Maximum feed velocity of 0603 capacitor and drive frequency

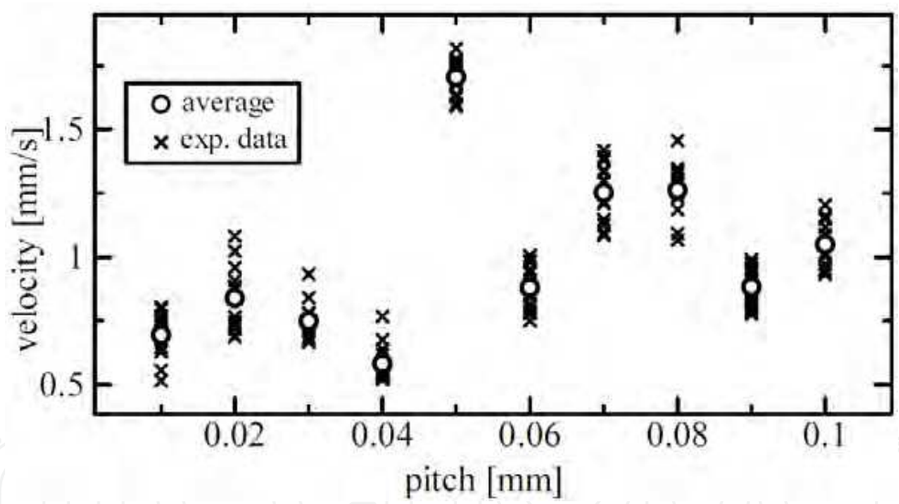

Fig. 10. Relationship between feeding velocity and sawtooth pitch

5. Analysis of 0603 capacitor

5.1 Measurement tools

As in the previous work (Mitani, 2006), the sawtooth surface profile should be selected according to the convexity size on the surface of the capacitor electrodes. To observe them, we used AZ-100 multi-purpose zoom microscope (Nikon Instruments Co.) (Figure 11), which can take pictures at up to 16 times magnification. The microscope also has an automatic stage to control focus height at a resolution of 0.54 μm. Each image is forwarded to a personal computer and saved as a bitmap file. We used DynamicEye Real focus image

synthesizing software (Mitani Corp.) to analyse these convexities. The software can synthesize a three dimensional (3D) model from these pictures according to focus height. Sections of the 3D model are analysed to obtain a convexity size and position.

Fig. 11. AZ-100 multi-purpose zoom microscope (Nikon Instruments Co.)

5.2 Convexity size and position

We assumed that each convexity on the electrodes of capacitor was defined as a half sphere. The radii of each convexity and its position were analysed from the 3D model. Analysing a synthesized model (Figure 12), we obtain a contour line of the synthesized model, defining the micropart coordinate G-xy (Figure 13). In this figure, the arrowed convexities could be disregarded because the convexities labelled as **A** occurred besides the capacitor, and the convexities labelled as **B** did not occur on any electrode of the capacitor. We thus defined four convexities on the surface of the 0603 capacitor.

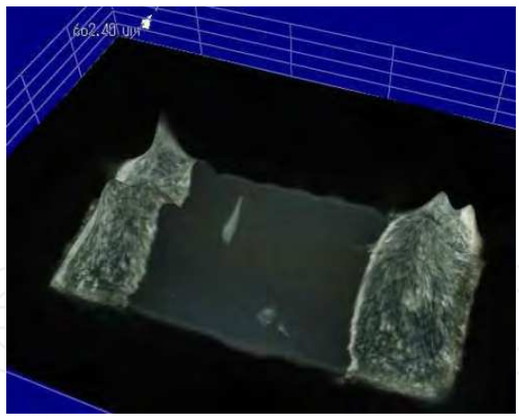

Fig. 12. Synthesized model of 0603 capacitor

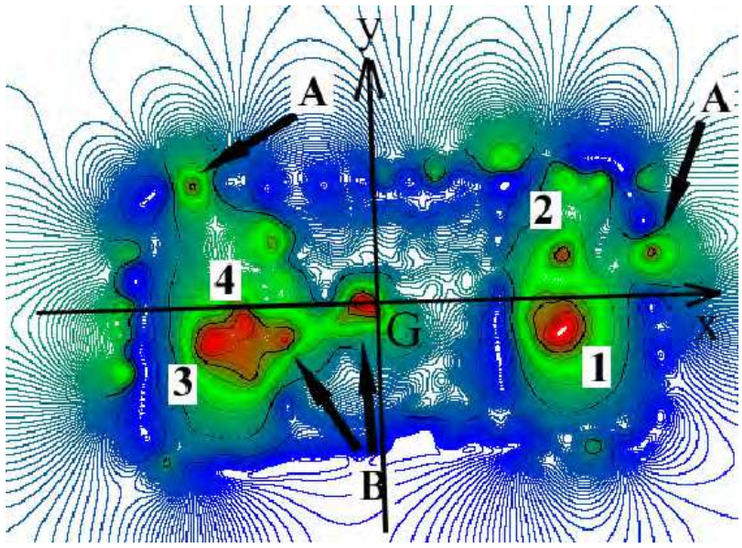

Fig. 13. Contour model

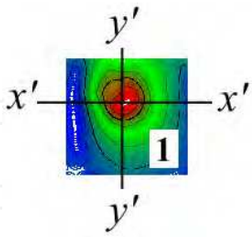

Fig. 14. Analysis line of convexity #1

Let us analyse convexity size from the 3D model. We first analysed the convexity #1 along a line x′x′ parallel to the x axis, and a line y′y′ parallel to the y axis, both lines pass the top of the convexity (Figure 14), and then we obtained two section models shown in Figure 15. Similarly, we analysed and obtained each section of convexities #2, #3, and #4, (Figures 16 to 18). Each convexity was approximated in a half sphere from the top to less than 18 μm. The radii of each convexity were assumed to be the mean value of radii along both directions.

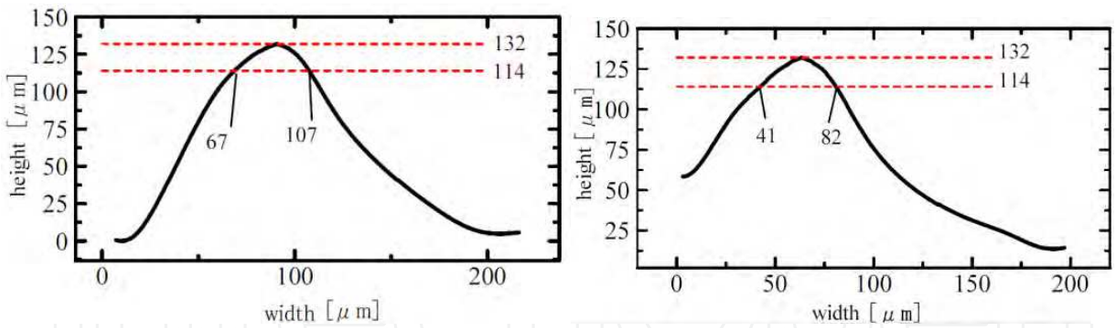

(a) along line x′x′ (b) along line y′y′

Fig. 15. Sections of convexity #1

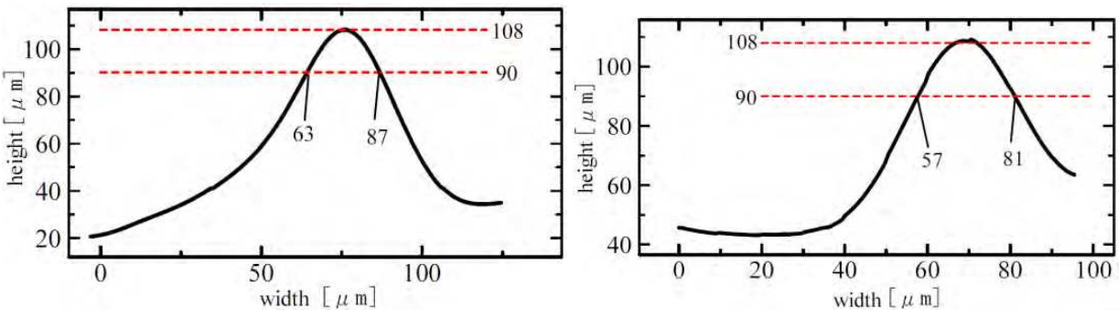

(a) along line x′x′ (b) along line y′y′

Fig. 16. Sections of convexity #2

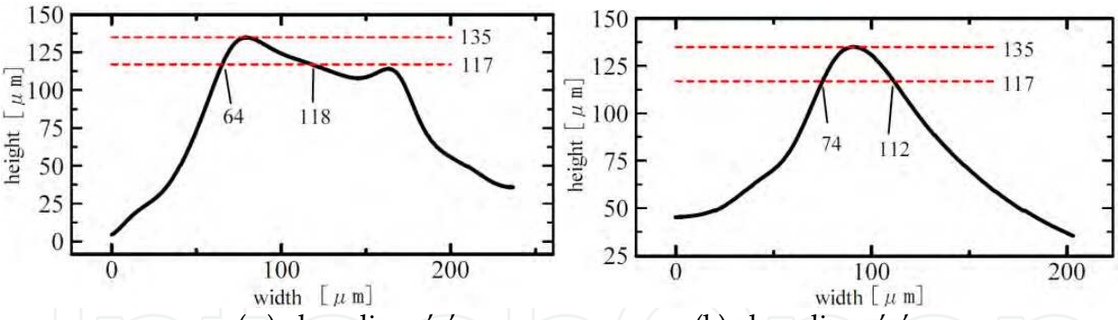

(a) along line x′x′ (b) along line y′y′

Fig. 17. Sections of convexity #3

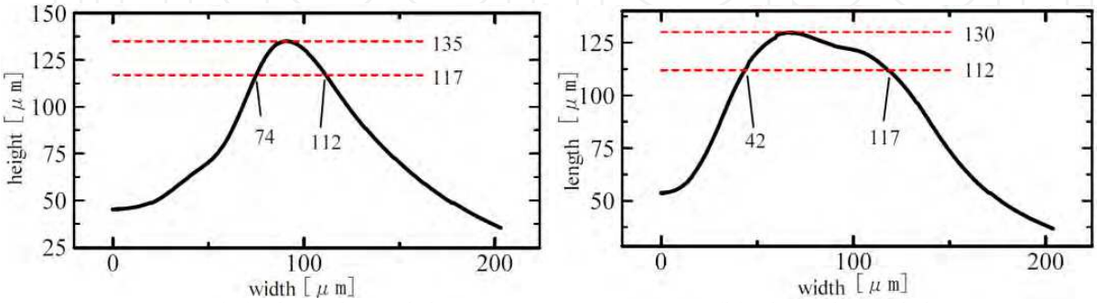

(a) along line x′x′ (b) along line y′y′

Fig. 18. Sections of convexity #4

From Figure 13, we measured position of each convexity with the top of each convexity on G-xy. Finally, we obtained convexity size and position appeared in Figure 13 (Table 2), and defined surface model of a 0603 capacitor (Figure 19).

no.	cordinate (x, y), μm	radus, μm
1	(207, -37)	20
2	(216, 51)	13
3	(-241, -36)	24
4	(-200, -6)	36

Table 2 Coordinate and radius of convexity

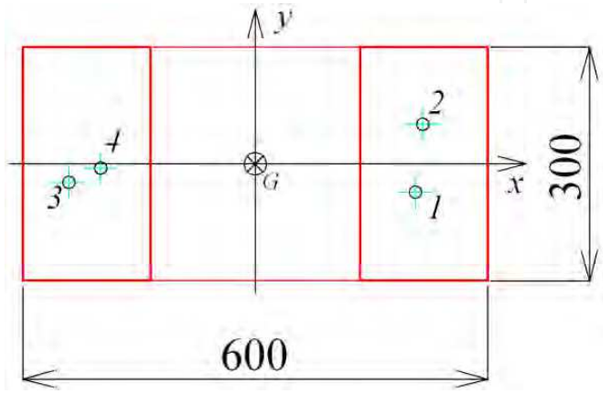

Fig. 19. Convexity model of 0603 capacitor

6. Feeding simulation and comparison

6.1 Feeding dynamics

We have already derived the dynamics of micropart when a convexity exists on the surface of micropart (Mitani, 2006). We extended these results to plural convexities. We defined the feeder coordinate O-x_0y_0 and micropart position and posture on its coordinate P = (x_c, y_c, φ).

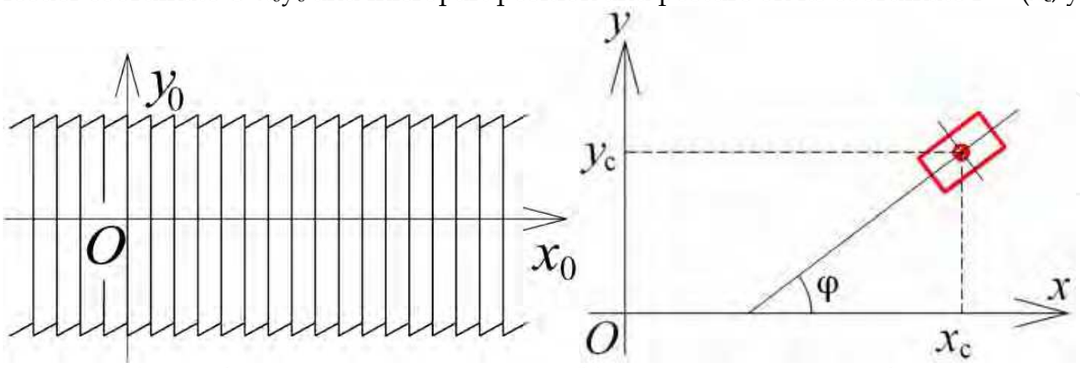

(a) coordinate (b) micropart position and posture

Fig. 20. Position of micropart on coordinate

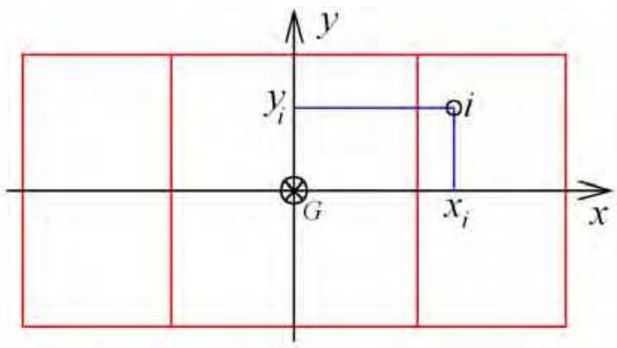

Fig. 21. Position of convexity i on the coordinate G-xy

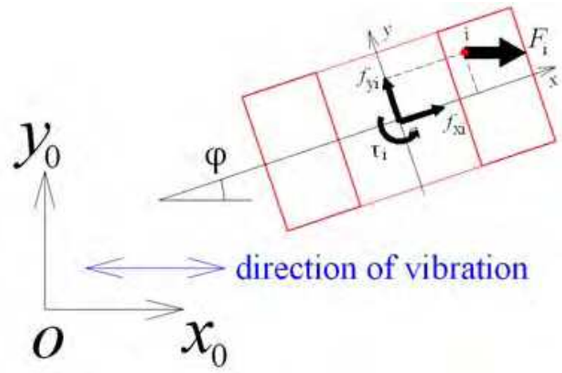

Fig. 22. Driving force of micropart transferred from convexity

We also defined potion of the i-th convexity as $c_i = (x_i, y_i)$ on the coordinate G-xy. Dynamics of micropart is represented as:

$$\begin{bmatrix} F_x \\ F_y \\ \tau \end{bmatrix} = \begin{bmatrix} m & 0 & 0 \\ 0 & m & 0 \\ 0 & 0 & I \end{bmatrix} \begin{bmatrix} \ddot{x}_c \\ \ddot{y}_c \\ \ddot{\varphi} \end{bmatrix} + \begin{bmatrix} c & 0 & 0 \\ 0 & c & 0 \\ 0 & 0 & d \end{bmatrix} \begin{bmatrix} \dot{x}_c \\ \dot{y}_c \\ \dot{\varphi} \end{bmatrix} \tag{1}$$

where m indicates mass of micropart, I intertia, c attenuation coefficients of motion, and d attenuation coefficients of rotation. Driving force and torque, $f \equiv (F_x, F_y, \tau)^T$, is calculated by the sum of driving force transferred from each convexity. Force generated by vibration of feeder surface occurs along direction of vibration. Considering the driving force $f_i \equiv (f_{xi}, f_{yi}, \tau_i)$ generated by contact force F_i, vibration force at i-th convexity shown in Figure 22, we found:

$$f_i = \begin{bmatrix} F_i \cos\varphi \\ -F_i \sin\varphi \\ -F_i \sqrt{x_i^2 + y_i^2} \sin(\varphi + \tan^{-1}(y_i / x_i)) \end{bmatrix} \tag{2}$$

Assuming that 1st, 2nd, …, and n-th convexities appear on the surface of a micropart, driving force f is represented as follows:

$$f = \sum_{i=1}^{n} f_i \tag{3}$$

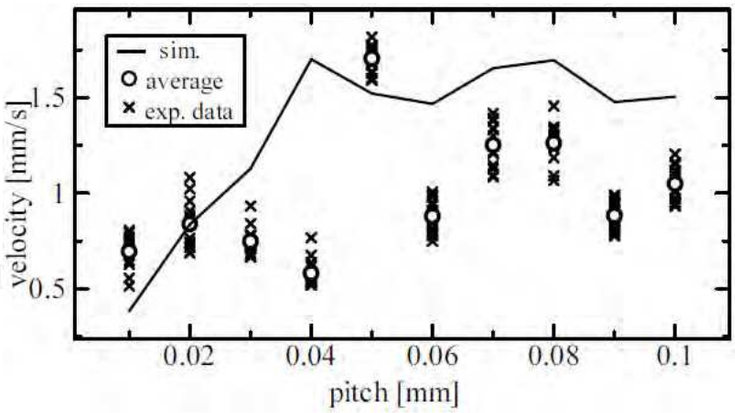

Fig. 23. Comparison of experimental and simulation results

6.2 Feeding simulation

In equation (2), each contact force F_i is decided according to its contact between a sawtooth and a convexity (Mitani, 2006). We conducted feeding simulation of the 0603 capacitor model shown in Figure 21, using the same parameters as feeding experiments, and then compared with experimental results (Figure 23). In the simulation, feed velocity peaked at p = 0.04 mm, whereas it peaked at p = 0.05 mm in the experiments. At the pitch of 0.01 to 0.04 mm, velocities were proportional to the sawtooth pitch. At the pitch of 0.07 to 0.1 mm, the experimental results were about 0.5 mm/s lower than simulation though the tendency was the same. Consequently, there were large differences between the simulation and experimental results. In the next section, we examine these differences by analyzing the micropart movement and feeder surface.

7. Examination of simulation error

7.1 Observation of micropart movement

We used Fastcam-1024PCI highspeed video camera (Photron) to capture micropart movement at 1000 fps. A 0603 capacitor was initially placed lengthwise on the feeder and the video camera was set to the side of the capacitor (Figure 24).

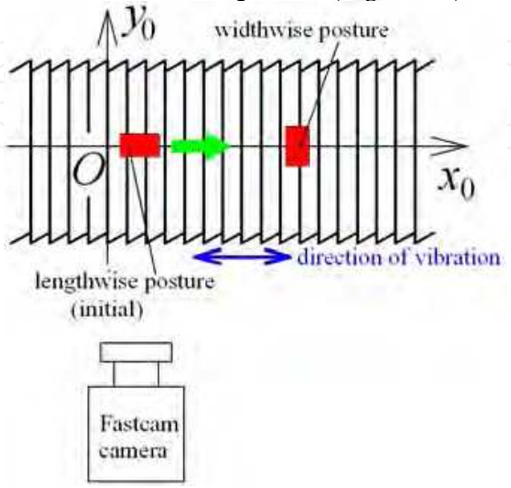

Fig. 24. Capture setup of micropart movement using a Fastcam video camera

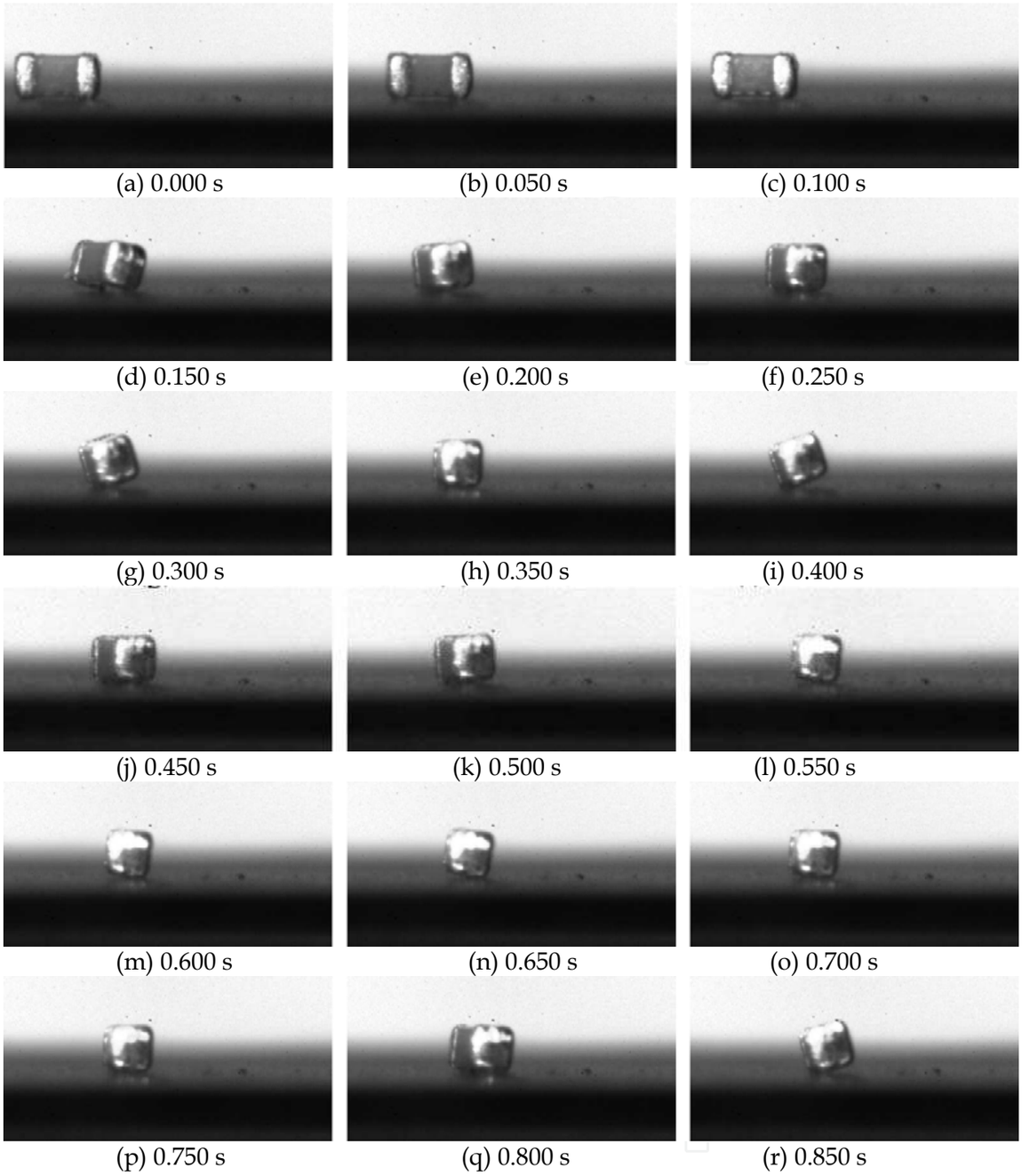

Fig. 25. Micropart movement

We obtained successive pictures of the capacitor movement from t = 0.000 to 0.850 s with an interval of 0.050 s (Figure 25). Beginning the feeder vibration at t = 0.000 s, the capacitor started to move along the feeder in the right direction upon feeder vibration. During the micropart moved in the right direction, the capacitor rotated around its vertical axis against the feeder surface (t = 0.150 s) and became oriented to widthwise at t = 0.300 s. When

moving along the feeder in this widthwise posture, the capacitor began to rotate around the y_0 axis. Rotation angles were 17° at t = 0.300 and 0.400 s, and -3° at t = 0.550 s.

7.2 Analysis of micropart rotation

Let us formulate this rotation at this widthwise posture. We added the z axis to the coordinate G-xy defined in Figure 19: the z axis is perpendicular to the xy plane (Figure 26). Considering the capacitor rotation around the point of contact when a tooth contacts a convexity C_i with contact force F_i, force F_τ, generated by torque τ_i, is represented as:

$$F_\tau = \frac{\tau_i}{r_i}, \qquad (r_i \equiv |C_1 G|) \tag{4}$$

If β is angle between C_1 G and y axis, force F′ along the y axis can be formulated as:

$$F' = F_i - F_\tau \cos\beta \tag{5}$$

This suggests that drive force reduces by rotation of the micropart. Consequently, we need to derive dynamics considering rotation to simulate the movement of microparts more accurately.

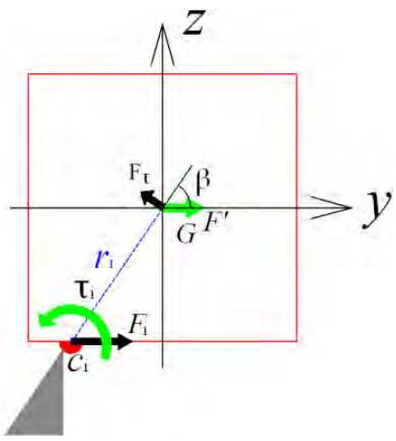

Fig. 26. Micropart rotation at widthwise posture

7.3 Analysis of feeder surface

Using the AZ-100 microscope (Figure 11), we obtained a synthesized model (Figure 27) and its contour model (Figure 28) of a sawtoothed surface. From these figures, feeder surface had many cracks and errors, not perfectly sawtoothed, which caused instable contact between the surface and a micropart, and affected the movement of micropart. Therefore, we need to formulate a feeder surface profile model based on measurements, and consider contact and adhesion using this model.

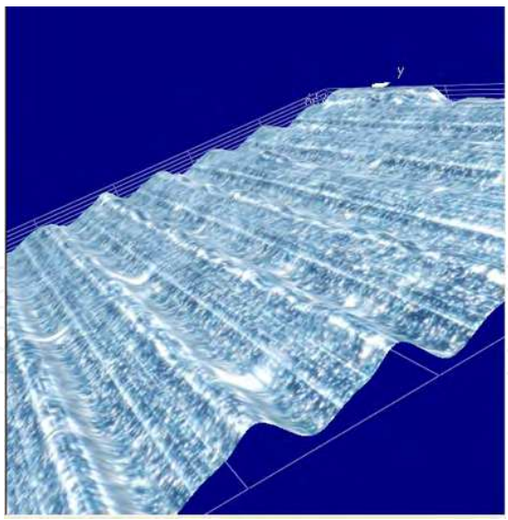

Fig. 27. Synthesized model of sawtoothed surface (p = 0.1 mm and θ=20 deg)

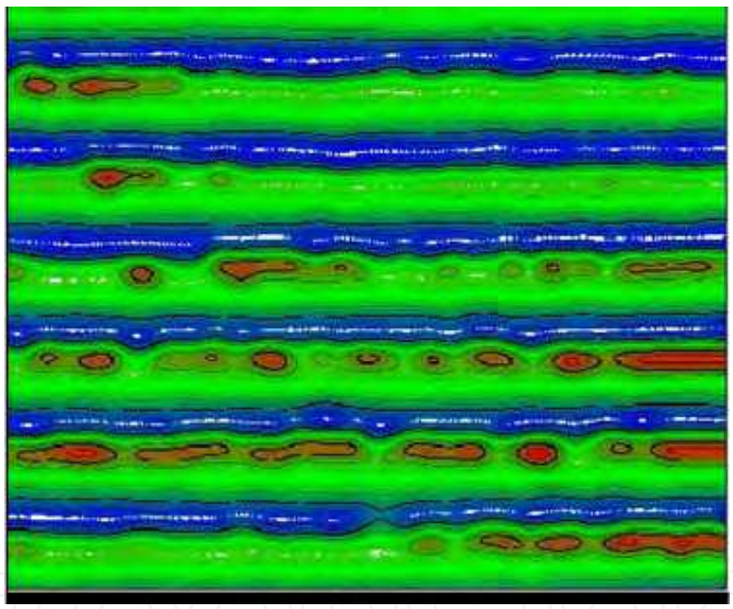

Fig. 28. Contour model

8. Conclusion

We examined a surface model of 0603 capacitor based on measurements. A microscope was used to analyse convexity sizes in the electrode surface. Each convexity was approximated as a half sphere model. These models were then applied for feeding simulation proposed in the previous work. Comparing with feeding experiments, we found large differences between the simulation and experimental results. We examined these differences by analyzing the movement of parts using a high speed video camera and found an error of oversight in our simulation. Capacitors rotated around the vertical axis against the sawtooth surface from a lengthwise to widthwise posture and continued to move along the feeder in

the desired direction while swinging around the axis along the sawtooth. This movement reduced the actual feeding velocity of a capacitor in contrast to the simulation. We also inspected a feeder surface profile using a microscope, and found many cracks and errors at the top of sawteeth, whereas feeder surface was perfectly sawtoothed in simulation. We concluded to need analysis of micropart rotation and a strict contact model between feeder surface and micropart based on measurements to simulate the feeding more accurately.
In future studies, we will try to:
· Identify dynamics of micropart including rotation,
· Formulate surface profile model of sawtoothed surface based on measurements, and analyse contact and adhesion using the model derived.
· Develop new feeder surfaces for smaller microparts, and,
· Verify the effect of ambient humidity on feeding.
This research was supported in part by a Grant-in-Aid for Young Scientists (B) (20760150) from the Ministry of Education, Culture, Sports, Science and Technology, Japan, and by a grant from the Electro-Mechanic Technology Advancing Foundation (**EMTAF**), Japan.

9. References

Mitani, A., Sugano, N. & Hirai, S.(2006). Micro-parts Feeding by a Saw-tooth Surface, *IEEE/ASME Transactions on Mechatronics*, Vol. 11, No. 6, 671-681.

Ando, Y. & Ino, J. (1997). The effect of asperity array geometry on friction and pull-off force, *Transactions of the ASME Journal of Tribology*, Vol. 119, 781-787.

Maul, G. P. & Thomas, M. B. (1997). A systems model and simulation of the vibratory bowl feeder, *Journal of Manufacturing System*, Vol. 16, No. 5, 309-314.

Wolfsteiner, P. & Pfeiffer, F. (1999). The parts transportation in a vibratory feeder, *Procs. IUTAM Symposium on Unilateral Multibody Contacts*, 309-318.

Reznik, D. & Canny, J. (2001). C'mon part, do the local motion!, *Procs. 2001 International Conference on Robotics and Automation*, Vol. 3, 2235-2242.

Berkowitz, D.R. & Canny, J. (1997), A comparison of real and simulated designs for vibratory parts feeding, *Procs. 1997 IEEE International Conference on Robotics and Automation,* Vol. 3, 2377-2382.

Christiansen, A. & Edwards, A. & Coello, C. (1996). Automated design of parts feeders using a genetic algorithm, *Procs. 1996 IEEE International Conference on Robotics and Automation*, Vol. 1, 846-851

Doi, T, (2001), Feedback control for electromagnetic vibration feeder (Applications of two-degrees-of-freedom proportional plus integral plus derivative controller with nonlinear element), *JSME International Journal*, Series C, Vol. 44, No. 1, 44-52.

Konishi, S. (1997). Analysis of non-linear resonance phenomenon for vibratory feeder, *Procs. APVC '97*, 854-859.

Fukuta, Y. (2004). Conveyor for pneumatic two-dimensional manipulation realized by arrayed MEMS and its control, *Journal of Robotics and Mechatronics*, Vol. 16, No. 2, 163-170.

Arai, M (2002). An air-flow actuator array realized by bulk micromachining technique, *Procs. IEEJ the 19th Sensor Symposium*, 447-450.

Ebefors, T. (2000), A robust micro conveyer realized by arrayed polyimide joint actuators, *Journal of Micromechanics and Microengineering*, Vol. 10, 337-349.

Böhringer, K.-F. (2003). Surface modification and modulation in microstructures: controlling protein adsorption, monolayer desorption and micro-self-assembly, *Journal of Micromechanics and microengineering*, Vol. 13, S1-S10.

Oyobe, H. & Hori, Y. (2001). Object conveyance system "Magic Carpet" consisting of 64 linear actuators-object position feedback control with object position estimation, *Procs. 2001 IEEE/ASME International Conference on Advanced Intelligent Mechatronics*, Vol. 2, 1307-1312.

Fuhr, G. (1999), Linear motion of dielectric particles and living cells in microfabricated structures induced by traveling electric fields, *Procs. 1999 IEEE Micro Electro Mechanical Systems*, 259-264.

Komori, M. & Tachihara, T. (2005). A magnetically driven linear microactuator with new driving method, *IEEE/ASME Transactions on Mechatronics*, Vol. 10, No. 3, 335-338.

Ting, Y. (2005), A new type of parts feeder driven by bimorph piezo actuator, *Ultrasonics*, Vol. 43, 566-573.

Codourey, A. (1995). A robot system for automated handling in micro-world, *Procs. 1995 IEEE/RSJ International Conference on Intelligent Robots and Systems*, Vol. 3, 185-190.

Mechatronic Systems Applications

Edited by Annalisa Milella Donato Di Paola and Grazia Cicirelli

ISBN 978-953-307-040-7
Hard cover, 352 pages
Publisher InTech
Published online 01, March, 2010
Published in print edition March, 2010

Mechatronics, the synergistic blend of mechanics, electronics, and computer science, has evolved over the past twenty five years, leading to a novel stage of engineering design. By integrating the best design practices with the most advanced technologies, mechatronics aims at realizing high-quality products, guaranteeing at the same time a substantial reduction of time and costs of manufacturing. Mechatronic systems are manifold and range from machine components, motion generators, and power producing machines to more complex devices, such as robotic systems and transportation vehicles. With its twenty chapters, which collect contributions from many researchers worldwide, this book provides an excellent survey of recent work in the field of mechatronics with applications in various fields, like robotics, medical and assistive technology, human-machine interaction, unmanned vehicles, manufacturing, and education. We would like to thank all the authors who have invested a great deal of time to write such interesting chapters, which we are sure will be valuable to the readers. Chapters 1 to 6 deal with applications of mechatronics for the development of robotic systems. Medical and assistive technologies and human-machine interaction systems are the topic of chapters 7 to 13.Chapters 14 and 15 concern mechatronic systems for autonomous vehicles. Chapters 16-19 deal with mechatronics in manufacturing contexts. Chapter 20 concludes the book, describing a method for the installation of mechatronics education in schools.

InTech Europe
University Campus STeP Ri
Slavka Krautzeka 83/A
51000 Rijeka, Croatia
Phone: +385 (51) 770 447

InTech China
Unit 405, Office Block, Hotel Equatorial Shanghai
No.65, Yan An Road (West), Shanghai, 200040, China
中国上海市延安西路65号上海国际贵都大饭店办公楼405单元
Phone: +86-21-62489820

Fax: +385 (51) 686 166
www.intechopen.com

Fax: +86-21-62489821

IntechOpen